The design and optical properties of orthosilicate phosphor-bredigite-like structure as a green light component in WLED device

Ha Thanh Tung[1], Nguyen Le Thai[2], My Hanh Nguyen Thi[3], Huynh Thanh Thien[4]
[1]Faculty of Basic Sciences, Vinh Long University of Technology Education, Vinh Long Province, Vietnam
[2]Faculty of Engineering and Technology, Nguyen Tat Thanh University, Ho Chi Minh City, Vietnam
[3]Faculty of Mechanical Engineering, Industrial University of Ho Chi Minh City, Ho Chi Minh City, Vietnam
[4]Faculty of Electrical and Electronics Engineering, Ton Duc Thang University, Ho Chi Minh City, Vietnam

Article Info

ABSTRACT

We produce the green phosphor $Ca_{14-x}Eu_xMg_2[SiO_4]_8$ (CEMSO) to be a part of the white light emitting diodes (WLEDs), short for diodes that generate white illumination. It has wide emission spectra, reaching highest value as 505 nm when excited at the wavelength of 400 nm, which is caused by the 4f 65d–4f 7 shift (excited state to ground state) in an ion of Eu^{2+}. The dipole-dipole interactivity appeared to be main energy shift method for the electric multipolar nature in CEMSO. We determine the critical distance to be 12.9 Å as well as 14.9 Å via a critical Eu^{2+} concentration and theory of Dexter regarding the energy shift. The CEMSO is integrated into the phosphor compound of yellow-phosphor/silicone for producing the UV-LED (395 nm). The impacts of CEMSO concentrations on UV-LED performances are determined. Significant improvements in chromatic uniformity and luminous output of the WLED are reported. The color rendering index (CRI) is not promoted, but this can be addressed by combining CEMSO green phosphor with red-luminescence materials, for example, red quantum dots or red phosphors.

Corresponding Author:

Huynh Thanh Thien
Faculty of Electrical and Electronics Engineering, Ton Duc Thang University
Ho Chi Minh City, Vietnam
Email: huynhthanhthien@tdtu.edu.vn

1. INTRODUCTION

The white light emitting diode (WLED) devices have been considerably recognized for their certain advantages, including power-economical feature, significant durability, limited impact in environment [1], [2]. On the other hand, there are existing limitations for WLEDs to widely utilized as an efficient lighting alternative to the standard fluorescent lights. It is possible to produce white illumination through coating the LED chip generating blue illumination with a yellow phosphor, commonly YAG:Ce^{3+}. This WLED package yields significant lumen efficacy reaching to almost 200 lm/W^{-1} [3], but it also yields inferior color rendering index (CRI) value because of the shortage of red-light element. Additionally, different from the phosphor YAG:Ce^{3+}, the majority of phosphors do not possess absorption band wide enough to match the excitation wavelength between 440 nm and 460 nm [4]. To overcome such limitation, researches have proposed a WLED version that possesses remarkable features of chromatic generation, surpassing the standard WLEDs [5]. There have been certain promising attempts at creating phosphors used for LED devices such as oxide [6], [7], oxyfluoride [8]–[10], nitride [11], [12], and oxynitride latticework [13], [14] excited under close-UV

light. However, it is essential to make further developments in phosphor materials for great performance, greater heat consistency, and chromatic features to meet the demands of quick development of solid state illuminating technology.

Among various phosphor bases, the alkaline earth silicate phosphor is an excellent option for improving the WLED quality because they offer remarkable heat consistency, chemical consistency as well as great performance [15]. According to a previous study, the bredigite $Ca_{14}Mg_2[SiO_4]_8$ (CMSO) possesses a strong absorption band under the near-UV or blue excitation, making it suitable for the white LED production [16]. Studies on CMSO as a phosphor host for rare-earth ion dopants were also conducted and demonstrated the significant enhancement in luminescence intensity [17], [18]; for example, the Eu^{2+}-activated CMSO exhibits strong green emission with luminescent improvement of ~142% [19]. Though the research on Eu^{2+}-activated CMSO was made, they focused on the structure and luminescence of the phosphor and barely discussed its effects on the WLED configuration. Thus, in this work, we utilized $Ca_{14-x}Eu_xMg_2[SiO_4]_8$ (CEMSO) phosphor to produce a WLED package. The influences of the phosphor's presence on the WLED lighting are monitored through varying the phosphor concentrations. The Eu^{2+} energy-shift mechanism is reviewed in section 2 with equations based on theory of Dexter. The examined WLED comprised of the InGaN LED chip with λ_{max} equal to 395 nm, YAG:Ce^{3+} phosphor, and Eu^{2+}-activated CMSO phosphor. The lighting features assessments include the color temperature uniformity, the luminosity, and chromatic rendering performance of the as-prepared WLED. Findings of this work show that the CEMSO enhances the WLED luminosity and color distribution homogeneity with its increasing concentration. The color rendition performance declines with higher CEMSO weight percentages, but this can be improved by combining with red-emission materials.

2. METHOD
2.1. Making $Ca_{14-x}Eu_xMg_2[SiO4]_8$ phosphor

We synthesised CEMSO in powder form via solid-phase reaction route. The materials used for the synthesis include $CaCO_3$, MgO, SiO_2, and Eu_2O_3 with high purity of 99.9%. The Eu concentration is constant at 0.3 mol% [18], [19]. All ingredients were mixed by grinding and subsequently subjected to a 4-hour heating phase at different temperatures in the range of 1373–1673 K under reducing atmosphere of 5%H_2-95%N_2. The room-temperature photoluminescence spectrum of the phosphor powder was determined with a luminescence spectrophotometer from Hitachi Co., Japan (Hitachi F-4500, 300-700 nm scanning wavelengths). The phosphor's quantum yield was obtained via the quantum efficiency measuring system of Otsuka electronics QE-1000 excited at the wavelength of 400 nm. For the measurement of the diffuse reflectance absorption spectrum, an UV-visible spectrophotometer from Varian manufacturer (the Cary 500, 200-600 nm) was applied [9], [20]–[22].

Our group prepared the LED apparatus through utilizing a composition containing CEMSO, yellow phosphor, and translucent silicone resin over the InGaN LED chip with λ_{max} equal to 395 nm, illustrated in Figure 1. To determine the electroluminescence, we put the separate LED apparatus built up on m-plane GaN over the silver headers linked with golden wires to form electric functioning. Afterwards, we covered the apparatus with a phosphor/silicone compound, positioned over the headers and cured afterwards. Following the procedure, we took measurements of the device within a sphere with DC bias forward current. We replicated the phosphor layer in the WLED's silicone films through LightTools 9.0 along with the Monte Carlo method. Two essential phases make up the recreation process. First, we must choose and prepare design samples with the desired lighting properties for WLED lights. Second, our team modifies CEMSO amounts to monitor the changes in the performance of prepared WLEDs. The examinations are monitored under different correlated color temperature (CCT) ranges of 3000-5000 K and 6000-8000 K.
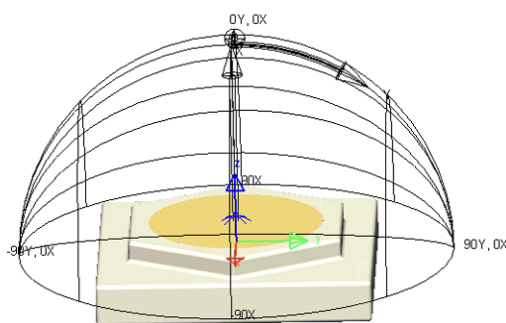

Figure 1. The WLED apparatus model built by using LightTools 9.0 with Monte Carlo method

2.2. Spectra optimization of the CCT

The close relationship between the peak location, the intensity of emission and the Eu^{2+} substitution can be demonstrated with the change in Eu concentration. As the concentration of Eu^{2+} goes up, the emission band with λ_{ex} equal to 400 nm moves to larger wavelength, which is caused by the reabsorption among the ions of Eu^{2+}, instead of the shifts in the crystal field surrounding Eu^{2+}, determined by the following formula [23]:

$$\Delta = Dq = \frac{Ze^2r^4}{6R^5} \qquad (1)$$

In the formula, Dq represents the crystal field with octahedral symmetry. R the ion's range of separation in the center and the ligand of the ion. Z represents the anion's charge or valence. e represents the electron's charge. r represents the d wavefunction's radius. The cutting of the crystal field, therefore, would not be the primary cause of red shift because of the ion radius for 8-coordinate Ca^{2+} being inferior to Eu^{2+} (1.12 Å compared to 1.25 Å). The most desirable concentration of the Eu^{2+} dopant was 0.3 mol%. More than 0.3 mol% of Eu in the phosphor composition could induce the reduction in the relative emission intensity, which is also known as the result of concentration quenching. It is possible to determine the energy shift's critical distance, represented by R_c, for the phosphor CEMSO using the structure-related parameters such as the unit's cell volume (signified via V), the amount of Eu^{2+} locations for each unit cell (represented by N) as well as the critical concentration (represented by X_c) [24]:

$$Rc \approx 2\left(\frac{3V}{4\pi X_c N}\right)^{1/3} \qquad (2)$$

In the formula, R_c indicates the disassociation among the nearest ions of Eu^{2+} at the critical distance. With V equal to 1356.5 Å, N equal to 8, X_c equal to 0.3, the Eu^{2+} critical shift distance for CEMSO would be roughly 12.9 Å. In addition, the Dexter theory is utilized to determine the shift for the electric dipole-dipole interactivity as the symmetry allowed shifts of Eu^{2+} are involved [24]. According to Blasse, R_c can be determined by the formula [25]:

$$PSA = \frac{2\pi}{h}|\langle S,A^*|H_{SA}|S^*,A\rangle|^2 \int g_s(E)g_A(E)dE \qquad (3)$$

$$R_c^6 = 0.63 \times 10^{28} \frac{4.8 \times 10^{-16}.P}{E^4} \int f_S(E)F_A(E)dE \qquad (4)$$

In the formulas, P represents oscillator power for the ion of Eu^{2+}. E represents energy for the maximal intersection of spectrum. $\int f_S(E)F_A(E)$ or the spectrum intersection integral, indicates the result for normalized spectrum forms for emission as well as excitation. The E and $\int f_S(E)F_A(E)$ results are attained via the information of spectrum displayed by Figure 2. In case of P respective to the wide $4f^7 => 4f^65d$ absorption band, we acquire the result of 10^{-2} [25], [26]. We acquire the E and $\int f_S(E)F_A(E)$ results through the spectrum, determined to be 2.66 eV and $1.88 \times 10^{-2}eV^{-1}$. From 4, we determined the R_c of the CMS:Eu^{2+} energy shift to be 14.9 Å.

3.   RESULTS AND DISCUSSION

Figure 2 shows that the proportion of the green phosphor CEMSO percentage to the yellow phosphor YAG:Ce^{3+} amount is reversed, which indicates that the mean CCT rates remain sustained. The variation of phosphor concentrations also promotes the scattering and absorption of the phosphor, resulting in the changes of chroma-distribution performance along with lumen output of the WLED device. In other words, by regulating the amount of CEMSO in the phosphor compound, the enhancement in better color coordination is achievable. The figure shows that increasing the CEMSO weight percentage (wt%) from 2 to 30, the YAG:Ce^{3+} wt% declines, especially when observed under CCT ranges 7000-8000 K. In the case of the lower CCT ranges of 3000-5000 K Figure 2(a), the YAG:Ce^{3+} concentration also decreases with the increase in CEMSO wt%, but the decrease is not as significant as that obtained under 6000-8000 K Figure 2(b). These findings indicate that the high wt% of CEMSO can boost the luminous output of the WLEDs with the CCT ranges $\geq$5000 K.
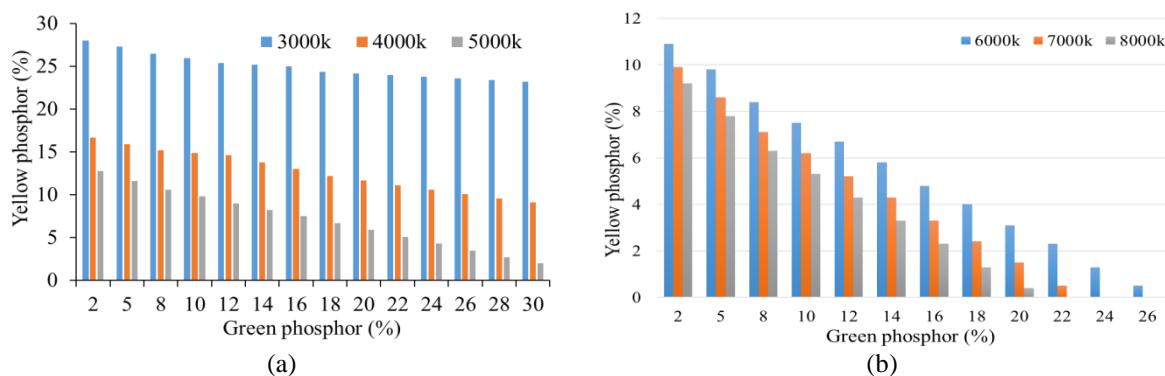
Figure 2. Adjusting the phosphor ratio to maintain the median CCT: (a) 3000-5000 K and (b) 6000-8000 K

The transmission band of WLEDs is affected by the integrating amount of the green phosphor CEMSO, as seen in Figure 3. The emission power of the WLED is monitored under two specific CCT levels of 6000 K Figure 3(a) and 8000 K Figure 3(b), and the concentration of CEMSO green phosphor varies from 2 wt% to 26 wt%. In both figures, increasing CEMSO concentrations stimulates the emission power in green-yellow region (~545-590 nm) while decreasing the emission peak intensity in blue region (~450 nm). The decrease in blue-emission peak intensity is more significant with the CCT preset of 6000 K. Besides, when the concentration of CEMSO phosphor increase, the emission peak shifts from yellow region (580 nm) to green region (545 nm). Such results are attributed to the efficient blue-light absorption and conversion of the CEMSO phosphor. Moreover, the higher CEMSO amount leads to the lower YAG:Ce^{3+} amount, leading to the shift of the emission peak from yellow to green regions. Additionally, the stronger blue and yellow-green emission intensities are noticed with the 8000-K CCT preset, implying that the CEMSO phosphor is capable of enhancing the luminosity of the WLED with high chroma temperature.
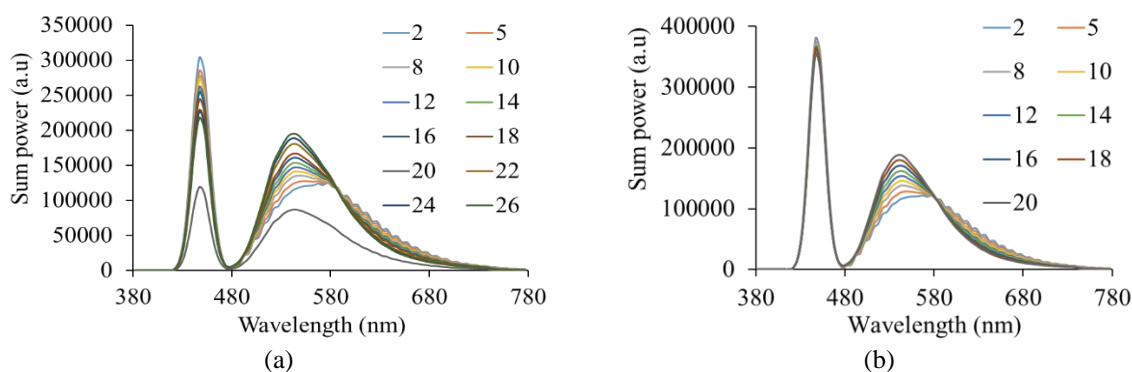

Figure 3. Emission peaks and distribution of generated white light with different CEMSO concentrations:
(a) 6000 K and (b) 8000 K

To validate the ability to enhance the WLED luminosity of the CEMSO phosphor, the lumen-output results are displayed in Figure 4. Here, two sets of CCT levels of 3000-5000 K Figure 4(a) and 6000-8000 K Figure 4(b) are taken into account, while the CEMSO phosphor wt% is from 2 to 30%. With increasing CEMSO amounts, the luminous flux intensity increases with all CCT levels, except the CCT presets of 3000 K and 4000 K. Particularly, with the higher concentration of the green phosphor, the luminous intensity at 3000 K slightly slips, while that at 4000 K is relatively stable. Meanwhile, at the other CCT presets, we can observe a great growth in the luminosity of the WLED apparatus. This can be attributed to the lower blue-light utilization when the yellow phosphor amount is still high. The high concentration of yellow phosphor can cause significant reabsorption of scattered blue and green light, which induces the transmission energy loss for the declining lumen output. Thus, the CEMSO phosphor proves to be appropriate for the WLED apparatus with the CCT presets larger than 5000 K.
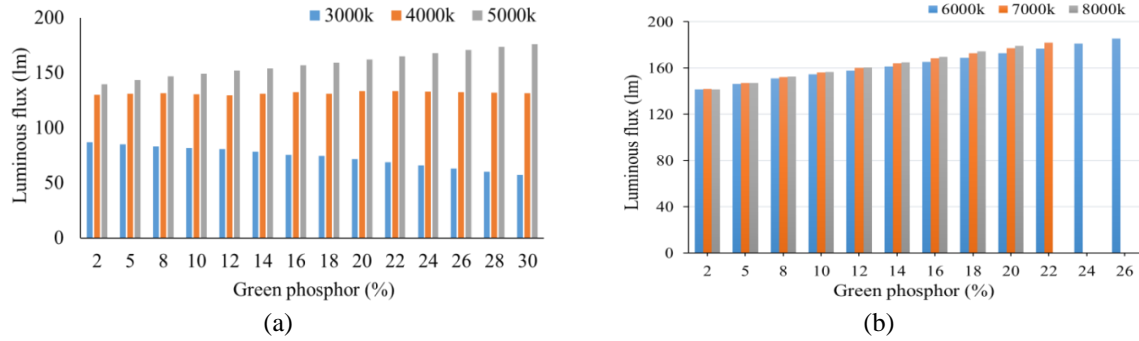
Figure 4. Luminosity of WLED apparatuses with different CEMSO concentrations: (a) 3000-5000 K and (b) 6000-8000 K

As the concentration of CEMSO varies, the distribution of light at different wavelengths changes. Referring to Figure 3, the emission peak shift from yellow to green is noticed, showing that the color variation levels possibly decline for a more uniform color spread on the chroma scale. The delta CCT, used to assess the color differences between the maximum and minimum CCT values at a specific CCT and CEMSO concentration, is determined and depicted in Figure 5. The notable fluctuation of delta CCT is noticed in the case of 3000-5000 K Figure 5(a). Meanwhile, the delta CCT monitored at 6000-8000 K gradually declines on the rising CEMSO amount see Figure 5(b). However, in general, the increase of CEMSO wt% reduces the color deviation in all CCT presets. The fluctuation in delta CCT under lower CCT preset can be attributed to the high reflection of converted light by high yellow-phosphor amount. Based on the findings, the CEMSO green phosphor is superior in enhancing the color uniformity high-CCT WLED packages, which is often regarded as a challenge in developing novel phosphor materials for LED devices.

The color rendering index (CRI) of the WLED with CEMSO green phosphor is also crucial. As expected, the increasing CEMSO concentration reduces the CRI, regardless of monitored CCT presets see Figure 6. However, considering the CRI between CCT levels at the same CEMSO concentration, 3000-5000 K in Figure 6(a) and 6000-8000 K in Figure 6(b), the higher CCT level exhibits the greater CRI value. This shows the potential of CEMSO in regulating the chromatic rendition efficiency at high color temperatures for the WLED model. To further discuss the CEMSO's chromatic rendition influence, the color quality scale (CQS), a more comprehensive parameter for chromaticity assessment, is utilized. The obtained CQS levels with various CEMSO amounts from 2 wt% to 30 wt% are depicted in Figure 7. The difference in CQS between two sets of CCT, from 3000-5000 K Figure 7(a) to 6000-8000 K Figure 7(b), is notable. In the low CCT preset, the CQS declines gradually, similar to the trend of the CRI. Nevertheless, the CQS monitored under higher CCT preset shows an increase before dropping. In particular, the CQS reaches its peak at the at the CEMSO concentration of 8 wt%, in 6000-8000 K. The CQS takes into account the CRI and color coordinating performance, thus the exhibited increase could be attributed to the lower CCT deviation (higher color uniformity). So, the green phosphor CEMSO proves its efficiency in improving the light emission uniformity and rendering performance. The high CRI requires red-light energy, so we can improve the CRI by combining the CEMSO with another commercial red phosphor; however, their concentrations must be adjusted to obtain the optimal results. Therefore, we will investigate such topics in future works.
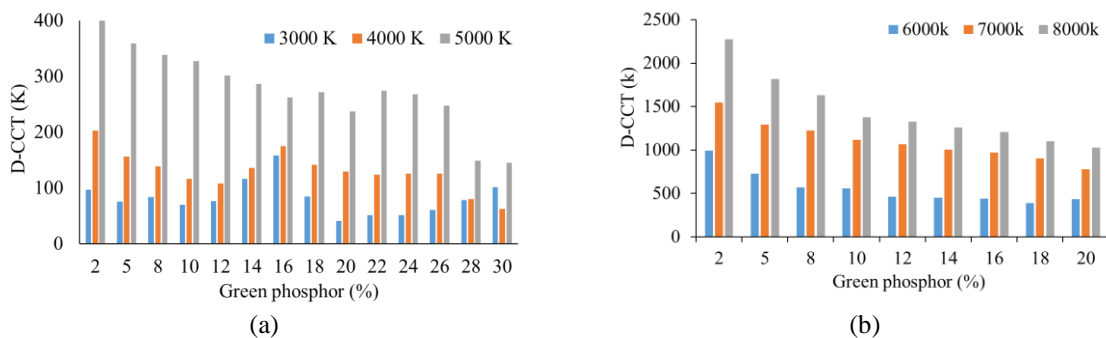

Figure 5. The delta CCT of WLED apparatuses with different CEMSO concentrations: (a) 3000-5000 K and (b) 6000-8000 K
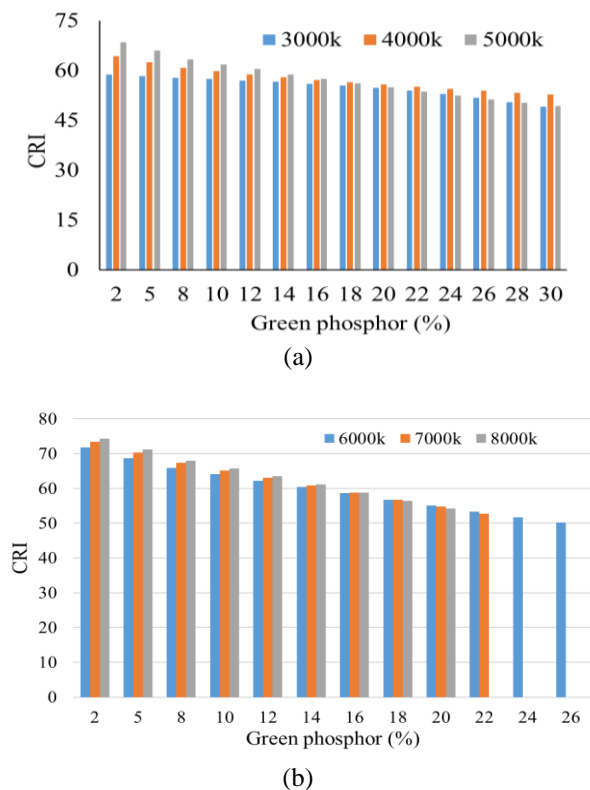
(a)

(b)

Figure 6. CRI levels of WLED apparatuses with different CEMSO concentrations: (a) 3000-5000 K and (b) 6000-8000 K
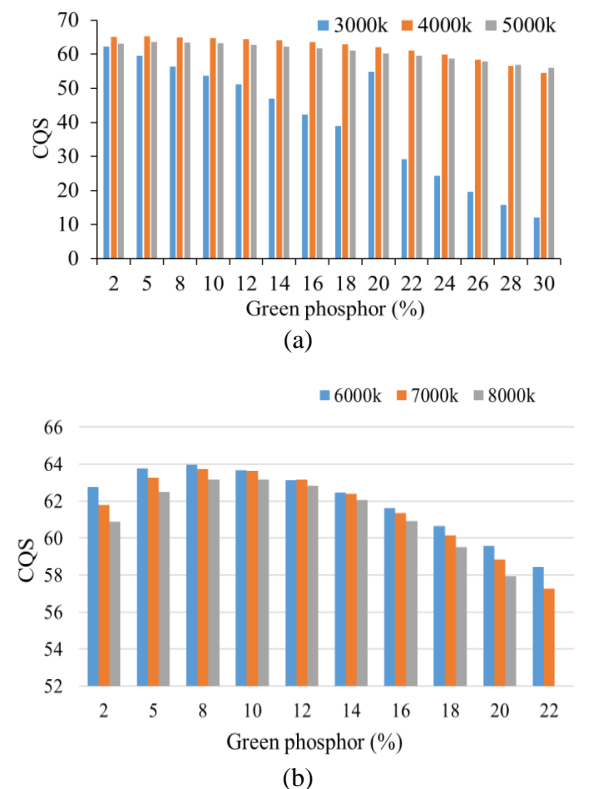

(a)

(b)

Figure 7. CQS levels of WLED apparatuses with different CEMSO concentrations: (a) 3000-5000 K and (b) 6000-8000 K

4.   CONCLUSION

The study herein demonstrates the green phosphor CEMSO produced using the solid state reaction with a fixed Eu concentration of 0.3 mol%. The CEMSO concentrations have noticeable influences on the WLED apparatuses. When increasing the green phosphor amounts, the emission peak shifts from yellow to green as the concentration of yellow phosphor declines. The green phosphor CEMSO proves its efficiency in improving the light emission uniformity and rendering performance. With 8 wt% of CEMSO, the CQS exhibits the highest value. The luminosity of the WLED shows improvement with higher CEMSO concentrations, especially in the 6000-8000 K CCT presets. However, the high CRI of the generated white light shows a reduction on the increasing CEMSO concentrations, due to the unresolved red-component shortage. The CEMSO phosphor can be used with other red phosphors to overcome this issue. Overall, according to results, the CEMSO green phosphor is effective in enhancing the WLED's illumination efficacy under high CCT ranges (>5000 K).

REFERENCES

[1]   C. Wu *et al.*, "Phosphor-converted laser-diode-based white lighting module with high luminous flux and color rendering index," *Optics Express*, vol. 28, no. 13, pp. 19085–19096, Jun. 2020, doi: 10.1364/OE.393310.

[2]   R. Dang, H. Tan, N. Wang, G. Liu, F. Zhang, and X. Song, "Raman spectroscopy-based method for evaluating LED illumination-induced damage to pigments in high-light-sensitivity art," *Applied Optics*, vol. 59, no. 15, pp. 4599–4605, May 2020, doi: 10.1364/AO.379398.

[3]   A. G. Bispo-Jr, L. F. Saraiva, S. A. M. Lima, A. M. Pires, and M. R. Davolos, "Recent prospects on phosphor-converted LEDs for lighting, displays, phototherapy, and indoor farming," *Journal of Luminescence*, vol. 237, p. 118167, Sep. 2021, doi: 10.1016/j.jlumin.2021.118167.

[4]   S. Ma, P. Hanselaer, K. Teunissen, and K. A. G. Smet, "Effect of adapting field size on chromatic adaptation," *Optics Express*, vol. 28, no. 12, pp. 17266–17285, Jun. 2020, doi: 10.1364/OE.392844.

[5]   D. Yan, S. Zhao, H. Wang, and Z. Zang, "Ultrapure and highly efficient green light emitting devices based on ligand-modified $CsPbBr_3$ quantum dots," *Photonics Research*, vol. 8, no. 7, pp. 1086-1092, Jul. 2020, doi: 10.1364/PRJ.391703.

[6]   A. Ali *et al.*, "Blue-laser-diode–based high CRI lighting and high-speed visible light communication using narrowband green-/red-emitting composite phosphor film," *Applied Optics*, vol. 59, no. 17, pp. 5197-5204, Jun. 2020, doi: 10.1364/AO.392340.

[7]   P. Kaur, Kriti, Rahul, S. Kaur, A. Kandasami, and D. P. Singh, "Synchrotron-based VUV excitation-induced ultrahigh quality cool white light luminescence from Sm-doped ZnO," *Optics Letters*, vol. 45, no. 12, pp. 3349–3352, Jun. 2020, doi: 10.1364/OL.395393.

[8]   F. Brusola, I. Tortajada, I. Lengua, B. Jordá, and G. Peris-Fajarnés, "Parametric effects by using the strip-pair comparison method around red CIE color center," *Optics Express*, vol. 28, no. 14, pp. 19966–19977, Jul. 2020, doi: 10.1364/OE.395291.

[9]   J.-O. Kim, H.-S. Jo, and U.-C. Ryu, "Improving CRI and Scotopic-to-Photopic Ratio Simultaneously by Spectral Combinations of CCT-tunable LED Lighting Composed of Multi-chip LEDs," *Current Optics and Photonics*, vol. 4, no. 3, pp. 247–252, 2020, doi: 10.1364/COPP.4.000247.

[10]   N. A. Mica *et al.*, "Triple-cation perovskite solar cells for visible light communications," *Photonics Research*, vol. 8, no. 8, pp. A16–A24, Aug. 2020, doi: 10.1364/PRJ.393647.

[11]   Y. Wang, G. Xu, S. Xiong, and G. Wu, "Large-field step-structure surface measurement using a femtosecond laser," *Optics Express*, vol. 28, no. 15, pp. 22946–22961, Jul. 2020, doi: 10.1364/OE.398400.

[12]   M. Abd Elkarim, M. M. Elsherbini, H. M. AbdelKader, and M. H. Aly, "Exploring the effect of LED nonlinearity on the performance of layered ACO-OFDM," *Applied Optics*, vol. 59, no. 24, pp. 7343–7351, Aug. 2020, doi: 10.1364/AO.397559.

[13]   G. E. Romanova, V. I. Batshev, and A. S. Beliaeva, "Design of an optical illumination system for a tunable source with acousto-optical filtering," *Journal of Optical Technology*, vol. 88, no. 2, pp. 66–71, Feb. 2021, doi: 10.1364/JOT.88.000066.

[14]   L. V. Labunets, A. B. Borzov, and I. M. Akhmetov, "Regularized parametric model of the angular distribution of the brightness factor of a rough surface," *Journal of Optical Technology*, vol. 86, no. 10, pp. 618–626, Oct. 2019, doi: 10.1364/JOT.86.000618.

[15]   Y. Liang *et al.*, "Phosphor-in-glass (PIG) converter sintered by a fast Joule heating process for high-power laser-driven white lighting," *Optics Express*, vol. 29, no. 10, pp. 14218–14230, May 2021, doi: 10.1364/OE.419633.

[16]   B. Wang, D. S. Li, L. F. Shen, E. Y. B. Pun, and H. Lin, "Eu^{3+} doped high-brightness fluorophosphate laser-driven glass phosphors," *Optical Materials Express*, vol. 9, no. 4, pp. 1749–1762, Apr. 2019, doi: 10.1364/OME.9.001749.

[17]   J. Zhang and C. Jiang, "Luminescence properties of $Ca_{14}Mg_2(SiO_4)8:Eu^{2+}$ from various Eu^{2+} sites for white-light-emitting diodes," *Materials Research Bulletin*, vol. 60, pp. 467–473, Dec. 2014, doi: 10.1016/j.materresbull.2014.08.054.

[18]   K. H. Lee, S. Choi, H.-K. Jung, and W. Bin Im, "Bredigite-structure $Ca_{14}Mg_2[SiO_4]_8:Eu^{2+},Mn^{2+}$: A tunable green–red-emitting phosphor with efficient energy transfer for solid-state lighting," *Acta Materialia*, vol. 60, no. 16, pp. 5783–5790, Sep. 2012, doi: 10.1016/j.actamat.2012.07.005.

[19]   K. H. Lee and W. Bin Im, "Efficiency Enhancement of Bredigite-Structure $Ca_{14}Mg_2[SiO_4]_8:Eu^{2+}$ Phosphor via Partial Nitrid," *Journal of the American Ceramic Society*, vol. 96, no. 2, pp. 503–508, Feb. 2013, doi: 10.1111/jace.12057.

[20]   L. Yang, Q. Zhang, F. Li, A. Xie, L. Mao, and J. Ma, "Thermally stable lead-free phosphor in glass enhancement performance of light emitting diodes application," *Applied Optics*, vol. 58, no. 15, pp. 4099–4104, May 2019, doi: 10.1364/AO.58.004099.

[21]   A. D. Corbett *et al.*, "Microscope calibration using laser written fluorescence," *Optics Express*, vol. 26, no. 17, pp. 21887–21899, Aug. 2018, doi: 10.1364/OE.26.021887.

[22]   Y. Zhang, X. Zhu, A. Liu, Y. Weng, Z. Shen, and B. Wang, "Modeling and optimizing the chromatic holographic waveguide display system," *Applied Optics*, vol. 58, no. 34, pp. G84–G90, Dec. 2019, doi: 10.1364/AO.58.000G84.

[23]   X. Shi, J. Liu, J. Xiao, and J. Han, "Design of a compact waveguide eyeglass with high efficiency by joining freeform surfaces and volume holographic gratings," *Journal of the Optical Society of America A*, vol. 38, no. 2, pp. A19–A26, Feb. 2021, doi: 10.1364/JOSAA.404280.

[24]   L. Li and M. J. Escuti, "Super achromatic wide-angle quarter-wave plates using multi-twist retarders," *Optics Express*, vol. 29, no. 5, pp. 7464–7478, Mar. 2021, doi: 10.1364/OE.418197.

[25]   S. Kashima *et al.*, "Wide field-of-view crossed Dragone optical system using anamorphic aspherical surfaces," *Applied Optics*,

vol. 57, no. 15, pp. 4171–4179, May 2018, doi: 10.1364/AO.57.004171.

[26] J. Chen, B. Fritz, G. Liang, X. Ding, U. Lemmer, and G. Gomard, "Microlens arrays with adjustable aspect ratio fabricated by electrowetting and their application to correlated color temperature tunable light-emitting diodes," *Optics Express*, vol. 27, no. 4, pp. A25–A38, Feb. 2019, doi: 10.1364/OE.27.000A25.

BIOGRAPHIES OF AUTHORS

Ha Thanh Tung received the Ph.D. degree in Physics from University of Science, Vietnam National University Ho Chi Minh City, Vietnam, he is working as a lecturer at the Faculty of Basic Sciences, Vinh Long University of Technology Education, Vietnam. His research interests focus on developing the patterned substrate with micro- and nano-scale to apply for physical and chemical devices such as solar cells, OLED, and photoanode. He can be contacted at email: tunght@vlute.edu.vn.

Nguyen Le Thai received his BS in Electronic Engineering from Danang University of Science and Technology, Vietnam, in 2003, MS in Electronic Engineering from Posts and Telecommunications Institute of Technology, Ho Chi Minh, Vietnam, in 2011 and Ph.D. degree of Mechatronics Engineering from Kunming University of Science and Technology, China, in 2016. He is a currently with the Nguyen Tat Thanh University, Ho Chi Minh City, Vietnam. His research interests include the renewable energy, optimisation techniques, robust adaptive control, and signal processing. He can be contacted at email: nlthai@ntt.edu.vn.

My Hanh Nguyen Thi received a Bachelor of Physics from An Giang University, Vietnam, Master of Theoretical Physics and Mathematical Physics, Hanoi National University of Education, Vietnam. Currently, she is a lecturer at the Faculty of Mechanical Engineering, Industrial University of Ho Chi Minh City, Vietnam. Her research interests are theoretical physics and mathematical physics. She can be contacted at email: nguyenthimyhanh@iuh.edu.vn.
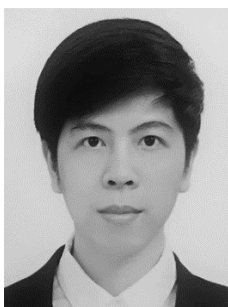
Huynh Thanh Thien received the Ph.D. degree in Electrical and Computer Engineering from the University of Ulsan, Ulsan, South Korea. He is working as a lecturer at the Faculty of Electrical and Electronics Engineering, Ton Duc Thang University, Ho Chi Minh City, Vietnam. His research interests include cognitive radio and next-generation wireless communications systems, game theory, deep learning, reinforcement learning, and semiconductor device. He can be contacted at email: huynhthanhthien@tdtu.edu.vn.